

Inverse iteration quantum eigensolvers assisted with a continuous variable

Min-Quan He,¹ Dan-Bo Zhang,^{2,3,*} and Z. D. Wang^{1,3,†}

¹*Department of Physics and HKU-UCAS Joint Institute for Theoretical and Computational Physics at Hong Kong, The University of Hong Kong, Pokfulam Road, Hong Kong, China*

²*Guangdong Provincial Key Laboratory of Quantum Engineering and Quantum Materials, GPETR Center for Quantum Precision Measurement and SPTE, South China Normal University, Guangzhou 510006, China*

³*Frontier Research Institute for Physics, South China Normal University, Guangzhou 510006, China*

The capacity for solving eigenstates with a quantum computer is key for ultimately simulating physical systems. Here we propose inverse iteration quantum eigensolvers, which exploit the power of quantum computing for the classical inverse power iteration method. A key ingredient is to construct an inverse Hamiltonian as a linear combination of coherent Hamiltonian evolution. We first consider a continuous-variable quantum mode (qumode) for realizing such a linear combination as an integral, with weights being encoded into a qumode resource state. We demonstrate the quantum algorithm with numeral simulations under finite squeezing, for a range of physical systems including molecules and quantum many-body models. We also discuss a hybrid quantum-classical algorithm that directly sums up Hamiltonian evolution with different durations for comparison. It is revealed that continuous-variable resources are valuable for reducing coherent evolution time of Hamiltonians in quantum algorithms.

I. INTRODUCTION

Solving eigenstates of many-body interacting Hamiltonian has caught a lot of attentions for past decades. Among many proposed quantum algorithms, two large groups are quantum phase estimation (QPE) [1] and variational quantum eigensolver (VQE) [2]. Remarkably, those two quantum algorithms exploit quantum resources in different strategies: QPE can estimate high accuracy eigenvalues with constant samples at a cost of large coherent circuit depth [3–7]; VQE can efficiently reduce the requirement of hardware coherent time with specified wavefunction ansatz, but at a price of increasing measurement repetitions for estimating observable [2, 8–11]. With but not limited to quantum eigensolvers as examples, trade-off between available quantum resources becomes an important theme in quantum algorithm designs.

The inverse power iteration (IPI) method is a standard numeral tool for solving eigenstates of quantum systems [12]. It is not scalable for large quantum systems, as time complexity of inverting Hamiltonian grows exponentially with system size due to the exponential growth of the dimension of Hilbert space [13]. Since a key ingredient is to perform an inverse operation on a Hamiltonian, it is natural to incorporate many developed quantum algorithms for matrix inversion [14–19] to endow quantum advantages for the IPI method. Nevertheless, the inverse matrix is in general non-unitary and its construction can be rather resource consuming. By expressing inverted Hamiltonian as an integral of Hamiltonian evolutions [20–22], a hybrid quantum-classical algorithm has been proposed recently using a summation of

Hamiltonian dynamics at discrete time [23], without referring to auxiliary qubits or qumodes and thus more feasible on near-term quantum devices. On the other hand, implementing quantum matrix inversion can be simplified with continuous-variable quantum modes (qumode), which naturally implements integral of unitaries without discretization [22, 24]. Along this line, we pursuit for a further simplified quantum algorithm with only one qumode to invert Hamiltonian. This makes the full quantum version of IPI method easier to implement, given that manipulation of qumode state and its coupling to qubits are highly controllable in some mainstream quantum platforms, e.g., superconducting circuits [25–27] and trapped ions [28–30]. Moreover, the valuable continuous-variable resource for solving eigenstates as well as other computational tasks may be revealed.

In this paper, we propose a quantum inverse power iteration (QuIPI) algorithm with single ancillary qumode for solving ground states and other eigenstates of quantum systems. The QuIPI involves inverting Hamiltonian as a key subroutine, which is constructed with linear combination of unitaries, with weights being encoded in a specified qumode resource state. We present a decomposition scheme of time evolution for coupled system-qumode Hamiltonian into basic quantum gates of qubits and one qubit-qumode gate. We numerically simulate the quantum algorithm for models ranging from quantum chemistry to quantum many-body systems, including molecular hydrogen, quantum Ising model and Kitaev ring. We also discuss a hybrid quantum-classical algorithm of IPI, where only evolution of system Hamiltonian with different evolution time is required. A comparison to QuIPI is made to stress the role of continuous-variable resource for reducing the requirement of long time evolution of the quantum system.

This paper is organized as follows. We firstly present the quantum algorithm in Sec. II. Then numerical results

* dbzhang@m.scnu.edu.cn

† zwang@hku.hk

of solving ground state energy are shown in Sec. III. Finally, conclusions and discussions are given in Sec. IV.

II. QUANTUM EIGENSOLVER

In this section, we formulate the QuIPI eigensolver. Firstly, we will introduce the inverse power iteration method and its quantum version, in which an efficient quantum algorithm for non-unitary matrix inversion plays an important role. Then we will present the whole procedure of ground state estimation, including initial state preparation, unitary evolution, and projection. Lastly, the time complexity of this algorithm will be analyzed.

A. Quantum version of inverse power iteration method

In the IPI method, the ground state of a given Hamiltonian \hat{H} is determined by iteratively performing inverse Hamiltonian \hat{H}^{-1} on an arbitrary initial state $|b\rangle^{(0)}$. The iteration is shown as

$$|b\rangle^{(k+1)} = \frac{\hat{H}^{-1}|b\rangle^{(k)}}{\|\hat{H}^{-1}|b\rangle^{(k)}\|}. \quad (1)$$

Here, a shift of energy is applied to keep all the eigenvalues positive to ensure the final state converges to an approximate ground state $|\psi_{g'}\rangle$ after K steps.

Since non-unitary operators are not natural on quantum computers, the non-unitary inverse matrix is represented as an integral of unitaries with ancillary qumodes [20–22, 24].

Adopting $a^{-1} = i \int_0^\infty e^{-iab} db$ from Fourier transformation, the inverse Hamiltonian can be expressed as

$$\hat{H}^{-1} = i \int_0^\infty e^{-i\hat{H}p} dp \quad (2)$$

Ideally, such a non-unitary operator can be obtained by performing an unitary operator $U = e^{-i\hat{H}\hat{p}}$ on both qubits $|b\rangle$ and a resource state ancillary qumode $|R\rangle = \int_0^\infty |p\rangle dp$ (not normalized), then projecting the ancillary qumode on zero position state $|q=0\rangle = \int_{-\infty}^\infty |p\rangle dp$. The result state $|\psi'\rangle$ is shown as

$$|\psi'\rangle = \langle q=0 | U | R \rangle |b\rangle = \int_0^\infty e^{-i\hat{H}p} |b\rangle dp = -i\hat{H}^{-1} |b\rangle \quad (3)$$

After K step iterations of above process, the final state converges to the approximate ground state $|\psi_{g'}\rangle$. Then the ground state energy E_0 is estimated by

$$\langle \psi_{g'} | \hat{H} | \psi_{g'} \rangle = E_0 + O((E_0/E_1)^{2K}), \quad (4)$$

where E_0 and E_1 are ground state energy and first excited state energy, respectively. This procedure can be

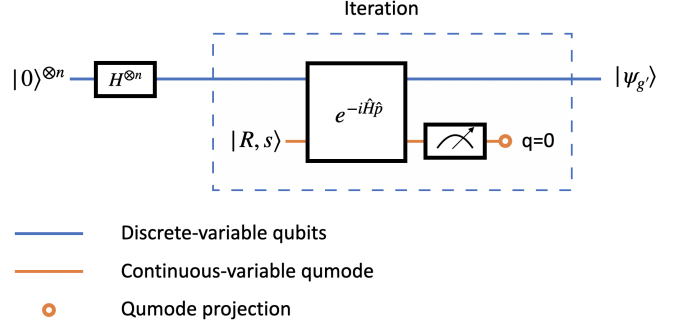


FIG. 1. Illustration of preparing the ground state for a Hamiltonian H with the QuIPI algorithm.

completed by quantum expectation estimation (QEE) [2] or SWAP test [31]. Eq. 4 shows the energy error results from inverse iteration exponentially decays with iteration step K (see Appendix A for more details.).

B. Procedure of quantum algorithm

We now present the algorithmic procedure of QuIPI for solving the ground state and estimating the ground state energy. While the algorithm has been illustrated under the infinite squeezing limit, we have to consider finite squeezing practically, both for the resource state preparation and the projection. For the initial state, inverse power iteration tells that it can not be orthogonal to the ground state [12]. We adopt an equal weighted state $|b\rangle^{(0)} = \frac{1}{\sqrt{2^N}} \sum_{n=0}^{2^N-1} |n\rangle$ as the initial state, while other choices also work. The quantum circuit is illustrated in Fig. 1, whose steps are as follows:

1. State preparation. We prepare the initial state of qubits as equally weighted state $|b\rangle^{(0)} = \frac{1}{\sqrt{2^N}} \sum_{n=0}^{2^N-1} |n\rangle$ by performing Hadmard gates on every qubit. The qumode is initialized in a finite squeezed resource state $|R, s\rangle = \sqrt{2}s^{-1/2}\pi^{-1/4} \int_0^\infty e^{-p^2/2s^2} |p\rangle dp$. By writing $|R, s\rangle$ in the Fock state space with a cutoff of Fock number, we can efficiently prepare the resource state, which is discussed in the Appendix. B.

2. Unitary operator performing. Performing a unitary operator $e^{-i\hat{H}\hat{p}}$ on both qubits and the ancillary qumode. The unitary operator can be decomposed as a set of universal single and two-qubit quantum gates and a qubit-qumode coupling gate $e^{-i\sigma^x \hat{p}}$, which will be given later.

3. Projection. Projecting the ancillary qumode on the finite squeezed position state $|q, s\rangle = s^{-1/2}\pi^{-1/4} \int_{-\infty}^\infty e^{-p^2/2s^2} |p\rangle dp$, the final state at

large s limit turns to be,

$$|\psi'\rangle = -i\sqrt{\frac{2}{\pi}}s^{-1}\sum_n(E_n^{-1} + O(s^{-2}))|\psi_n\rangle. \quad (5)$$

When $s \rightarrow \infty$, it recovers to the ideal case in Eq. 3. For the general case, a concrete expression is given in Appendix. C.

The procedure should be repeated K times. In each iteration, only if the ancillary qumode is successfully projected on the target state, the procedure continues; and remarkably, the qumode is re-prepared in the resource state $|R, s\rangle$. A factor s^{-1} in Eq. 5 accounts for the successful projection rate, implying that large squeezing factor leads to more accurate solution but lower success rate.

After successfully preparing the approximate ground state $|\psi_{g'}\rangle$, the last step is to estimate the ground state energy by QEE [2], in which expectation value of Hamiltonian is decomposed into several expectation of local operators,

$$E_0 = \langle\psi_{g'}|\hat{H}|\psi_{g'}\rangle = \sum_{l=1}^L c_l \langle\psi_{g'}|H_l|\psi_{g'}\rangle, \quad (6)$$

where \hat{H}_l is a tensor product of pauli matrices $\hat{H}_l = \otimes_{i=1}^N \sigma^{(i)}$ with $\sigma^{(i)} \in \{\sigma_x, \sigma_y, \sigma_z, I_2\}$, c_l is the corresponding weight, N is the number of qubits, and L is a polynomial of system size. We individually measure expectation value of each local operator $\langle\psi_{g'}|H_l|\psi_{g'}\rangle$ by local measurements of each qubit [32], then weighted sum up to obtain the ground state energy E_0 .

C. Time complexity analysis

We briefly analyze the time complexity. Firstly, recalling the error results from inverse power iteration is $O(r^{2K})$, where $r = E_0/E_1$ is ratio of ground energy and first excited energy. For desired energy accuracy ϵ , $K = O(\frac{\log \epsilon}{2\log r})$ step iteration is required. In practice, K can be very small.

Next is the error from Suzuki-Trotter decomposition. The unitary operator $e^{-i\hat{H}\hat{p}}$ is decomposed into several quantum gates on the circuit by trotter decomposition [33].

The unitary operator is expressed as the following form,

$$e^{-i\hat{H}\hat{p}} = (\prod_{l=1}^L e^{-ic_l\hat{H}_l\hat{p}/n})^n + O\left(\frac{1}{n}\right), \quad (7)$$

where each element $e^{-ic_l\hat{H}_l\hat{p}/n}$ can be constructed by a single qubit-qumode operator $e^{-i\sigma_x\hat{p}}$ and some qubit gates (see Appendix D). The state error is $O(\frac{1}{n})$ with n step of decomposition introducing an energy error of $O(\frac{1}{n^2})$. For a desired state accuracy ϵ' , total gates required are $O(L^3 c_{max}^2 / \epsilon')$ [34], which means

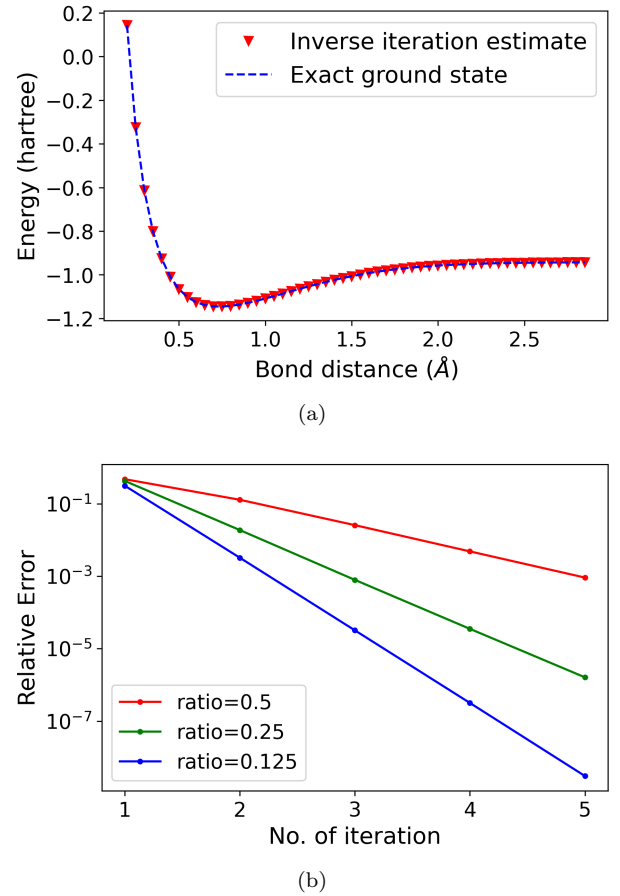


FIG. 2. (Color online) Solving ground state energy of H_2 . (a) Energy of H_2 at different bond distance. The blue dashed line is exact energy solved by diagonalizing the hydrogen molecular Hamiltonian. The red marker is solved by our quantum algorithm. (b) The relative error $|E_{exact} - E_{result}|/E_{exact}$ after every iteration for three chosen ratio of ground energy and first excited energy. The red line, green line and blue line correspond to the ratio being equal to 0.5, 0.25 and 0.125.

$O(L^3 c_{max}^2 / \sqrt{\epsilon})$ gates are required in each iteration for desired energy accuracy ϵ . Totally, there are $O(KL^3 c_{max}^2 / \sqrt{\epsilon})$ quantum gates in the quantum circuit.

The repetition times required is also analyzed. Considering finite squeezed, the error is proportional to s^{-2} , as evaluated from Eq. 5. So, the energy error is $O(s^{-4})$. For a desired energy error ϵ , squeezing factor is $O(\epsilon^{-1/4})$. As we mentioned, the successful projection rate is $O(s^{-1})$. For K step iteration, the total repetition time is $O(s^K) = O(\epsilon^{-K/4})$ for state preparation. Then, $O(c_{max}^2 L \epsilon^{-2})$ times measurements are required by using QEE [2]. The number of total samples is $O(c_{max}^2 L \epsilon^{-(2+K/4)})$. In total, the runtime for solving ground state energy is

$$O(L^4 c_{max}^4 K \epsilon^{-(5/2+K/4)})$$
 for requisite accuracy ϵ .

III. NUMERICAL RESULTS

In this section, we simulate the QuIPI for several models, including molecular hydrogen, quantum Ising model and Kitaev ring. They are the standard models of quantum chemistry, many-body spin system and many-body fermionic model, respectively. This simulation is based on *QuTip* [35]. The numerical results show: 1. converge rate increases as the ratio of first excited energy and ground energy increases, and iteration step can be very small for an appropriate chosen shift of energy; 2. the energy error is proportional to negative quadratic step of Suzuki-Trotter decomposition n^{-2} , fitting the theoretical expectation; 3. phase transition can be well demonstrated by QuIPI.

Hydrogen molecular. Following Ref. [36] that transform the H_2 Hamiltonian to a spin system by binary tree transformation, we use two qubits to simulate the molecular hydrogen. The effective Hamiltonian presented by Pauli operators are constructed at different bond distance with parameters from Ref. [10], which can be expressed as,

$$H(\lambda) = c_0(\lambda)\mathcal{I} + c_1(\lambda)\sigma_1^z + c_2(\lambda)\sigma_2^z + c_3(\lambda)\sigma_1^z\sigma_2^z + c_4(\lambda)\sigma_1^x\sigma_2^x + c_5(\lambda)\sigma_1^y\sigma_2^y. \quad (8)$$

We set the squeezing factor $s = 10$, the highest Fock state being considered = 40, and iteration step $K = 5$ to estimate ground state energy. The bond dissociation is shown in Fig. 2(a). The estimated ground energy is perfectly fitted the exact one.

Then the relation between converge rate and ratio of first excited energy and ground energy is investigated. Fixing bound distance at 0.75Å, the ground energy and first excited energy equal to $-1.15E_h$ and $0.45E_h$. The ratio of first excited energy and ground energy equals to 2, 4, and 8 by applying shift of energy, $2.74E_h$, $1.68E_h$, and $1.37E_h$. Fig. 2(b) shows the relative error $|E_{exact} - E_{result}|/E_{exact}$ after every iteration for all the three cases. The result shows that higher ratio corresponds to the faster converge rate. Moreover, for ratio equals 0.25, after only 3 iterations the estimate energy has an extremely high accuracy, higher than 99.9%.

Quantum Ising model with transverse field. In one-dimensional quantum Ising model, the interaction of sites is presented as a tensor product of Pauli-Z operators performing on the two interacted neighboring sites and transverse field is expressed as a Pauli-X operator performing on the single site [37]. The Hamiltonian is

$$H = \sum_{i=1}^N a_i \sigma_i^x + \sum_{i=1}^N \sum_{j=1}^{i-1} J_{ij} \sigma_i^z \sigma_j^z, \quad (9)$$

where N is the number of sites (qubits), J is interaction strength between sites, and a is the external transverse field strength.

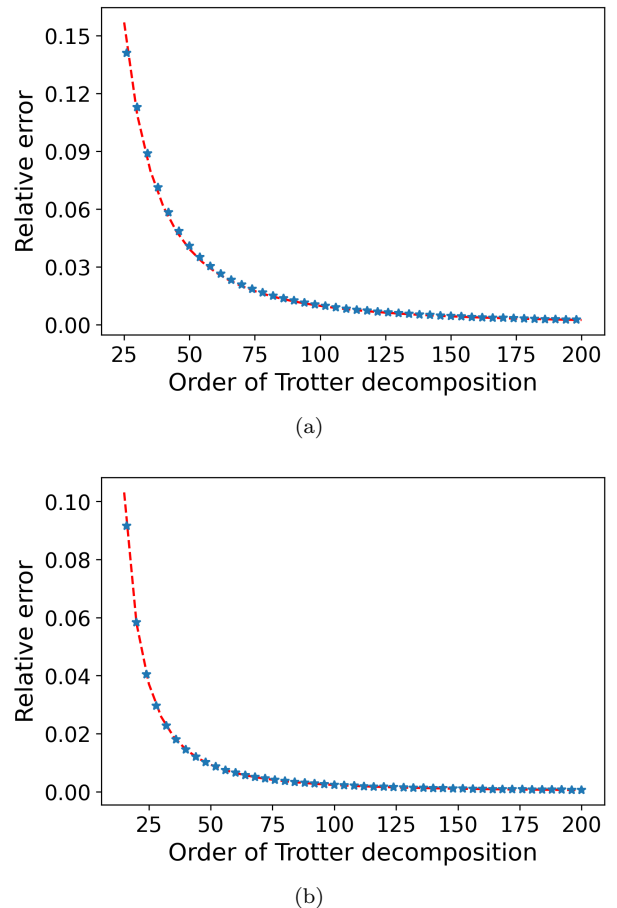
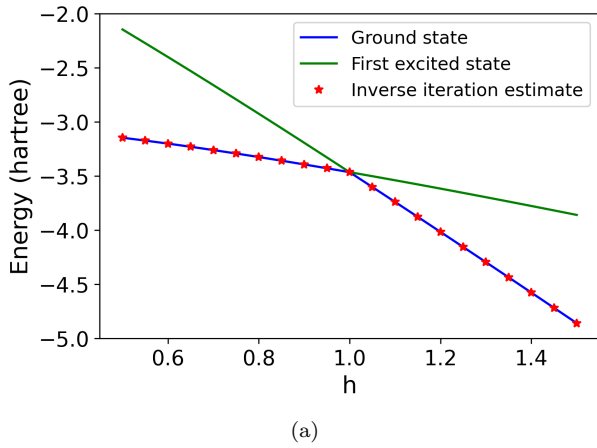


FIG. 3. Solving ground state energy of quantum Ising model with transverse field. The blue solid line is relative error of the energy estimated by our quantum algorithm $|E_{estimate} - E_{exact}|/E_{exact}$ and the red dashed line is the fitting curve that is proportional to $1/n^2$. The results of $n < 25$ are plotted in the embedded graph. (a) all the parameters a_i and J_{ij} are one. (b) the parameters are randomly sampled from 0 to 1 with an uniform distribution.

We use three qubits to solve ground state energy of quantum Ising model with transverse field. Two cases are considered: 1. all the parameters equal to one; 2. all the parameters are randomly chosen from an uniform distribution [0, 1]. In this part, we analyze the relation between the relative error and step of Suzuki-Trotter decomposition. The result is shown in Fig. 3, in which the blue star are relative errors at different step n and red dashed line is the fitting function that is proportional to $1/n^2$, meeting theoretical expectation mentioned in Sec. II C.

The Kitaev ring. The Kitaev ring is an one-dimensional fermion system that can be used to demonstrate quantum phase transition [38]. The Hamiltonian is

$$H = -J \sum_{i=1}^N (c_i^\dagger c_{i+1} + c_i^\dagger c_{i+1}^\dagger + h.c.) - \mu \sum_{i=1}^N c_i^\dagger c_i. \quad (10)$$



(a)

FIG. 4. (Color online) Solving ground state energy of Kitaev model. The blue line and green line are the exact ground state energy and first excited state energy, and red star is the energy estimated by our quantum algorithm. At $h = 1$, quantum phase transition happens.

Mapped to spin form by Jordan-Wigner transformation [39], it is presented as

$$H = -h \sum_{i=1}^N \sigma_i^z - J \sum_{i=1}^{N-1} \sigma_i^x \sigma_{i+1}^x - J \sigma_1^y (\prod_{i=2}^{N-1} \sigma_i^z) \sigma_N^y. \quad (11)$$

This model with $J = 1$ and changing h is simulated by three qubits. Fig. 4 shows the exact ground energy, first excited energy, and the result energy solved by our quantum algorithm. At $h = 1$, the quantum phase transition is well illustrated.

IV. DISCUSSION AND CONCLUSION

So far, we have focused on solving the ground eigenstate and ground state energy. However, the QuIPI and hybrid quantum-classical strategy can solve not only the ground state energy, but also the whole energy spectrum. As we mentioned, the result state of iterative power iteration method corresponds to the minimum absolute eigenvalue. So, we can determine any energy level by applying a shift of energy near the target energy. In this situation, the energy ratio mentioned in the time complexity should be replaced by the ratio of the target energy and the second minimum absolute energy.

Our algorithm takes the advantage of continuous-variable resources. To show it, we take a comparison between the QuIPI and the hybrid quantum-classical IPI that does not use the continuous-variable qumode. The hybrid one realizes inverse Hamiltonian by performing a series of unitary operators with different evolution time, i.e., $H^{-1} \approx \sum_{j=0}^{M_j-1} e^{-iH_j \Delta p} \Delta p$, where Δp is the discrete interval of the summation, and M_j is the up limit of the

summation (see Appendix E for details as well as numeral results for hydrogen molecular). This form implies that the hybrid quantum-classical IPI demands for long-time evolution of H , namely t in e^{-iHt} should be large enough. In comparison, the QuIPI refers to a qumode to encode weights of different unitaries into the resource state. As the resource state naturally has distribution for large quadrature \hat{p} , long-time evolution of the Hamiltonian is intrinsically realized with a coupling between the system and the qumode in terms of $e^{-iH\hat{p}}$. This comparison shows that the continuous-variable resource used in QuIPI can reduce the demanded coherence evolution time.

We briefly discuss the physical implementation of the quantum algorithm, since pursuing the advantage of continuous-variable in QuIPI relies on a hybrid-variable quantum platform for physical implementation. We note that the mainstream platforms of quantum computers based on qubits, such as trapped ions and superconducting circuits, often have continuous variables that couple with qubits. The physical implementation is very similar to Ref. [40] utilizing an auxiliary qumode, which is feasible for current quantum platforms, in the sense that all necessary components are readily implementable, including preparing the resource state $|R, s\rangle$, implementing $e^{-iH\hat{p}}$ and projection.

In summary, we have proposed inverse iteration quantum eigensolvers for solving eigenstates of Hamiltonian, which utilizes a continuous variable qumode to realize inverse Hamiltonian as an integral of Hamiltonian evolution. We have demonstrated the efficiency and accuracy of the QuIPI for a range of quantum systems including both quantum chemistry and quantum many-body models. We also have proposed a hybrid quantum-classical algorithm of IPI, where the integral is discretized and unitaries are summed classically. Compared with QuIPI, the hybrid algorithm relies longer time for Hamiltonian evolution. Lastly, we point out that quantum algorithm developed here may also be applied for matrix-inversion based quantum machine learning.

V. ACKNOWLEDGEMENTS

We thank Guo-Qing Zhang for helpful discussions. This work was supported by the CRF of Hong Kong (No. C6005-17G), the National Natural Science Foundation of China (Grants No. 91636218 and No. U1801661), the National Key Research and Development Program of China (Grant No. 2016YFA0301800), the Key Project of Science and Technology of Guangzhou (Grant No. 201804020055), and the Key-Area Research and Development Program of GuangDong Province (Grant No. 2019B030330001).

Appendix A: Energy error result from inverse iteration

The initial state can be rewritten as a superposition state of eigenstates of \hat{H}

$$|b\rangle = \sum_i b_i |\psi_i\rangle \quad (\text{A1})$$

with

$$\hat{H}^{-1} |\psi_i\rangle = E_i^{-1} |\psi_i\rangle. \quad (\text{A2})$$

So, performing k times \hat{H}^{-1} on initial state $|b\rangle$ leads to

$$|\psi_{g'}\rangle = \hat{H}^{-k} |b\rangle = \frac{1}{\sqrt{c}} \sum_i b_i E_i^{-k} |\psi_i\rangle \quad (\text{A3})$$

with normalization factor $1/\sqrt{c}$.

The expectation value of \hat{H} is

$$\begin{aligned} \langle \hat{H} \rangle &= \langle \psi_{g'} | \hat{H} | \psi_{g'} \rangle \\ &= \frac{1}{c} \sum_{i,j} b_i b_j E_i^{-k} E_j^{-k} \langle \psi_i | \hat{H} | \psi_j \rangle \\ &= \frac{1}{c} \sum_i b_i^2 E_i^{-2k} E_i \\ &= \frac{1}{c} (b_0^2 E_0^{-2k+1} + b_1^2 E_1^{-2k+1} + \dots) \\ &= \frac{1}{c} E_0^{-2k} [b_0^2 E_0 + b_1^2 (\frac{E_0}{E_1})^{2k} E_1 + \dots] \\ &= E_0 + O((\frac{E_0}{E_1})^{2k}) \end{aligned} \quad (\text{A4})$$

Appendix B: Demonstration of resource state preparation

We demonstrate the finite squeezed resource state qumode preparation by iteratively applying coherent displacement operator and phonon creation operator [41].

We firstly rewrite our resource state as a superposition state of Fock states:

$$|R, s\rangle = \sum_{n=0}^{\text{cut}} c_n |n\rangle, \quad (\text{B1})$$

where cut is the highest Fock state we consider, the weights c_n is transformed from the resource state in momentum space $c_n = \sqrt{2s^{-1/2}\pi^{-1/4}} \int_0^\infty e^{-p^2/2s^2} \langle n|p \rangle dp$ with $\langle n|p \rangle = i^n \pi^{-1/4} \frac{1}{\sqrt{2^n n!}} H_n(p) e^{-p^2/2}$, where $H_n(p)$ is Hermite polynomials.

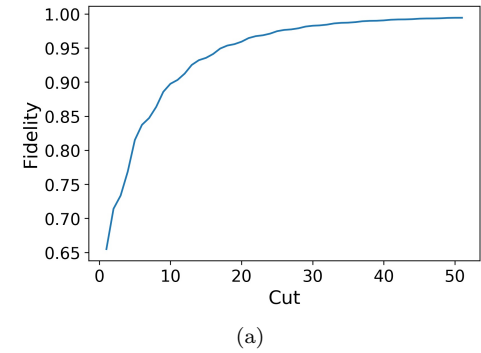
The target state can be achieved by

$$|R, s\rangle = \Pi_{n=1}^{\text{cut}} \hat{D}(\alpha_n) \hat{a}^\dagger \hat{D}(\alpha_n)^\dagger |0\rangle, \quad (\text{B2})$$

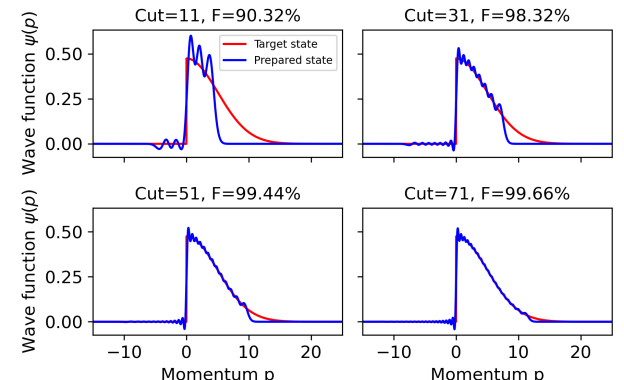
Where $\hat{D}(\alpha_n)$ is coherent displacement operator, \hat{a}^\dagger is creation operator, and $\{\alpha_n\}$ is determined by

$$\sum_{n=0}^{\text{cut}} \frac{c_n}{\sqrt{n!}} (\alpha^*)^n = 0. \quad (\text{B3})$$

We simulate this process to prepare our qumode resource state with squeezing factor equal five $|R, s=5\rangle$. Fig. 5(a) shows increasing cut can increase the fidelity of result qumode state. Fig. 5(b) shows the momentum distribution for four chosen cut.



(a)



(b)

FIG. 5. Qumode resource state preparation. (a) The fidelity between the target state and the state we prepared by the method that alternately applying the coherent displacement operator and creation operator. (b) The momentum wave function of the prepared qumode state with four chosen cut and the target momentum wave function.

Appendix C: Finite squeezing effect

Squeezed states are obtained by squeezing the qumode probability distribution on the position (momentum) space and extending it on the momentum (position) space. In this process, the qumode state conforms to the uncertainty principle from beginning to end. In Sec. II A, the qumode states are infinitely squeezed states. The projection qumode state $|q=0\rangle = \int_{-\infty}^{\infty} |p\rangle dp$ is infinitely squeezed on the position space and extended

on the momentum space, so that it has a certain position $q = 0$ but momentum is equally distributed from negative infinity to positive infinity. The resource state $|R\rangle = \int_0^\infty |p\rangle dp$ is infinitely squeezed on position space too, but only have positive momentum. In this case, the successful projection rate is zero. Moreover, infinite squeezed states can not experimentally obtained. For these two reasons, we have to consider finite squeezed states: $|q, s\rangle = s^{-1/2} \pi^{-1/4} \int_{-\infty}^\infty e^{-p^2/2s^2} |p\rangle dp$ and $|R, s\rangle = \sqrt{2} s^{-1/2} \pi^{-1/4} \int_0^\infty e^{-p^2/2s^2} |p\rangle dp$.

Considering the finite squeezed state, the result state after unitary operator performed and projection is

$$\begin{aligned} |\psi'\rangle &= \langle q, s | e^{-i\hat{H}\hat{p}} |R, s\rangle |b\rangle \\ &= \sqrt{2} s^{-1} \pi^{-1/2} \sum_n b_n \int_0^\infty e^{-iE_n p} e^{-p^2/s^2} dp |\psi_n\rangle \\ &= \frac{\sqrt{2}}{2} \sum_n b_n e^{-E_n^2 s^2/4} [1 - i \cdot \text{Erfi}(\frac{E_n s}{2})] |\psi_n\rangle, \end{aligned} \quad (\text{C1})$$

where Erfi is imaginary error function. The Taylor-series expansion at $s \rightarrow \infty$ of above equation is

$$|\psi'\rangle = -i \sqrt{\frac{2}{\pi}} s^{-1} \sum_n (E_n^{-1} + O(s^{-2})) |\psi_n\rangle, \quad (\text{C2})$$

where $\sqrt{\frac{2}{\pi}} s^{-1}$ is successful projection rate. Only in this case, the result is the desired state. And the error of final state is proportional to s^{-2} .

Appendix D: Arbitrary qubit-qumode quantum gate construction

In this part, we will discuss how to construct arbitrary qubit-qumode unitary operator $e^{-i\hat{H}_l\hat{p}}$, where \hat{H}_l is a tensor product of Pauli matrices and \hat{p} is the momentum operator. Starting from one qubit situation, we firstly show that all the four Pauli matrices can be transformed from a Pauli X matrix. For convenience, we denote $X = \sigma_x$, $Y = \sigma_y$, $Z = \sigma_z$, and $I = I_2$.

$$HXH = Z, SXS^\dagger = Y, XX = I \quad (\text{D1})$$

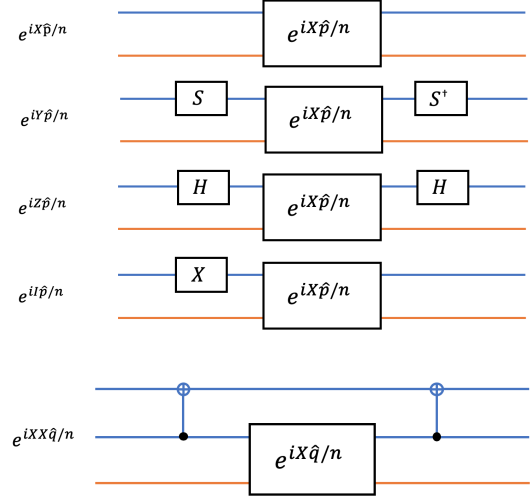
The one-qubit-one-qumode unitary operator can be realized by the following quantum circuit.

For more than one qubits situation, we use Controlled-NOT (CNOT) gate to entangle the qubits.

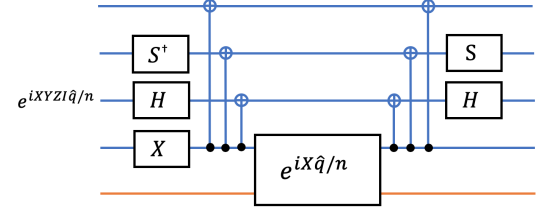
$$CNOT_{1,2}(X_1 \otimes I_2)CNOT_{1,2} = X_1 \otimes X_2, CNOT \quad (\text{D2})$$

where $CNOT_{1,2}$ is a CNOT gate controlled by the 1st qubit, targeting to the 2nd qubit.

So, two-qubits-one-qumode unitary operator $e^{iX_1 X_2 \hat{q}/n}$ can be implemented by the combination of $e^{iX\hat{q}/n}$ and a CNOT gate.



By using the two-qubit CNOT gate that entangles the qubits, and single qubit gate that transforms the Pauli X operator to other Pauli operators, we can construct an evolution operator of tensor product of arbitrary Pauli operators $e^{-i\hat{H}_l\hat{p}}$. The following quantum circuit is a good example.



Appendix E: Hybrid quantum-classical method

In this part, we propose a hybrid quantum-classical strategy of IPI that without any ancillae and thus post-selection. The inverse Hamiltonian is still expressed by linear combination of unitaries [23], but it is realized as a summation classically. Concretely, the inverse Hamiltonian is presented as a summation of evolution operators with different time, i.e., $H^{-1} \approx \sum_{j=0}^{M_j-1} e^{-iH_j \Delta p} \Delta p$, where Δp is the discrete interval of the summation, and M_j is the up limit of the summation. The maximal evolution phase is defined as $\phi_{max} = M_j \Delta p$.

For higher order, the inverse Hamiltonian is approximated as

$$\begin{aligned} H^{-k} &\approx \sum_{j_1=0}^{M_{j_1}-1} \cdots \sum_{j_k=0}^{M_{j_k}-1} e^{-iH_{j_1} \Delta p} \cdots e^{-iH_{j_k} \Delta p} \cdot \Delta p^k \\ &= \sum_J U(J) \cdot \Delta p^k. \end{aligned} \quad (\text{E1})$$

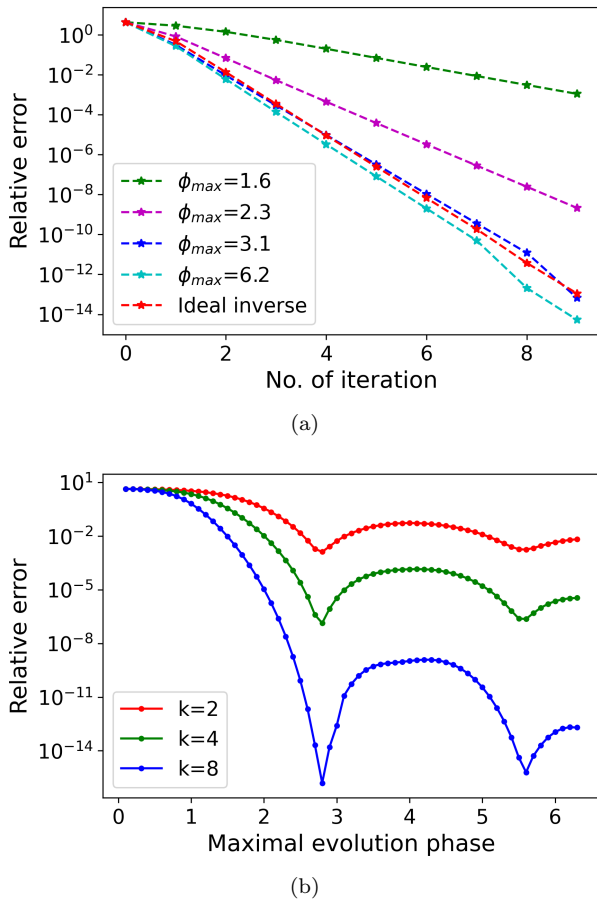


FIG. 6. (Color online) Solving ground state energy of hydrogen molecular with the bond distance being equal to 0.75 by the hybrid quantum-classical algorithm. (a) For a chosen maximal evolution phase ϕ_{max} , the relationship between the relative error $|E_{\text{estimate}} - E_{\text{exact}}|/E_{\text{exact}}$ and number of iteration k . The red line is the result with using the ideal inverted Hamiltonian H^{-1} . (b) For a chosen number of iteration k , the relationship between the relative error and maximal evolution phase ϕ_{max} .

The target state is evolved to $|\psi\rangle = H^{-k}|b\rangle \approx \sum_J U(J) \cdot \Delta p^k |b\rangle$. Then the ground state energy is expressed as

$$E \approx \sum_J \sum_{J'} \Delta p^{2k} \langle b|U(J)^\dagger H U(J')|b\rangle. \quad (\text{E2})$$

Each expectation value can be parallelly computed by SWAP test [31] or QEE [2], then summed up with corresponding weights to estimate the ground state energy.

We simulate the process of this method to solve H_2 at the situation that bond distance equal 0.75Å. In Eq. E2, there is a multiple summation leading to the time complexity exponentially increases with $2k$. To simplify the computation in our simulation, the high order inverse Hamiltonian is approximated by directly multiplying the first order one. The process is shown as

$$E = \langle b| \left(\left(\sum_{j=0}^{M_j-1} e^{-iHj\Delta p} \Delta p \right)^k \right)^\dagger H \left(\sum_{j=0}^{M_j-1} e^{-iHj\Delta p} \Delta p \right)^k |b\rangle. \quad (\text{E3})$$

The results obtained by Eq. E2 and Eq. E3 have been checked same at small k .

We set the discrete interval $\Delta p = 0.1$. For four chosen maximal evolution phase ϕ_{max} , the relation between relative error and number of iteration k is shown in Fig. 6(a). For fixed number of iteration k , the relative error at different maximal evolution phase ϕ_{max} is shown in Fig. 6(b).

In this hybrid quantum-classical strategy, matrix inversion is realized by a series of unitary operators with different evolution time from 0 to $(M_j - 1)\Delta p$. Considering Trotter decomposition, the number of gates required of unitary evolution increases with square of time [34]. For this reason, long time evolution leads to high circuit coherent time requirement and long total runtime. By comparison, QuIPI does not have this concern, since the linear combination of unitaries in QuIPI is assisted by qumode resource state and an evolution of $H\hat{p}$ with a fixed time period $t = 1$.

[1] A. Y. Kitaev, arXiv: 9511026 (1995).
[2] A. Peruzzo, J. McClean, P. Shadbolt, M.-H. Yung, X.-Q. Zhou, P. J. Love, A. Aspuru-Guzik, and J. L. O'brien, Nat. Commun. **5**, 4213 (2014).
[3] B. P. Lanyon, J. D. Whitfield, G. G. Gillett, M. E. Goggin, M. P. Almeida, I. Kassal, J. D. Biamonte, M. Mohseni, B. J. Powell, M. Barbieri, *et al.*, Nat. Chem. **2**, 106 (2010).
[4] J. Du, N. Xu, X. Peng, P. Wang, S. Wu, and D. Lu, Phys. Rev. Lett. **104**, 030502 (2010).
[5] B. M. Hoffman, D. Lukyanov, Z.-Y. Yang, D. R. Dean, and L. C. Seefeldt, Chem. Rev. **114**, 4041 (2014).
[6] A. Aspuru-Guzik, A. D. Dutoi, P. J. Love, and M. Head-Gordon, Science **309**, 1704 (2005).
[7] N. Wiebe and C. Granade, Phys. Rev. Lett. **117**, 010503 (2016).
[8] M.-H. Yung, J. Casanova, A. Mezzacapo, J. McClean, L. Lamata, A. Aspuru-Guzik, and E. Solano, Sci. Rep. **4**, 3589 (2014).
[9] J. R. McClean, J. Romero, R. Babbush, and A. Aspuru-Guzik, New J. Phys. **18**, 023023 (2016).
[10] P. J. O'Malley, R. Babbush, I. D. Kivlichan, J. Romero, J. R. McClean, R. Barends, J. Kelly, P. Roushan, A. Tranter, N. Ding, *et al.*, Phys. Rev. X **6**, 031007 (2016).
[11] D.-B. Zhang and T. Yin, Phys. Rev. A **101**, 032311 (2020).
[12] E. Pohlhausen, J. Appl. Math. Mech. **1**, 28 (1921).
[13] F. Le Gall, in *Proceedings of the 39th international symposium on symbolic and algebraic computation* (2014) pp.

296–303.

[14] A. W. Harrow, A. Hassidim, and S. Lloyd, *Phys. Rev. Lett.* **103**, 150502 (2009).

[15] B. D. Clader, B. C. Jacobs, and C. R. Sprouse, *Phys. Rev. Lett.* **110**, 250504 (2013).

[16] P. Rebentrost, M. Mohseni, and S. Lloyd, *Phys. Rev. Lett.* **113**, 130503 (2014).

[17] M. Schuld, I. Sinayskiy, and F. Petruccione, *Phys. Rev. A* **94**, 022342 (2016).

[18] I. Kerenidis and A. Prakash, arXiv:1603.08675 (2016).

[19] G. Wang, *Phys. Rev. A* **96**, 012335 (2017).

[20] H.-K. Lau, R. Pooser, G. Siopsis, and C. Weedbrook, *Phys. Rev. Lett.* **118**, 080501 (2017).

[21] J. M. Arrazola, T. Kalajdzievski, C. Weedbrook, and S. Lloyd, *Phys. Rev. A* **100**, 032306 (2019).

[22] D.-B. Zhang, S.-L. Zhu, and Z. D. Wang, *Phys. Rev. Lett.* **124**, 010506 (2020).

[23] O. Kyriienko, *Npj Quantum Inf.* **6**, 1 (2020).

[24] D.-B. Zhang, Z.-Y. Xue, S.-L. Zhu, and Z. D. Wang, *Phys. Rev. A* **99**, 012331 (2019).

[25] A. Wallraff, D. I. Schuster, A. Blais, L. Frunzio, R.-S. Huang, J. Majer, S. Kumar, S. M. Girvin, and R. J. Schoelkopf, *Nature* **431**, 162 (2004).

[26] H. Paik, D. Schuster, L. S. Bishop, G. Kirchmair, G. Catelani, A. Sears, B. Johnson, M. Reagor, L. Frunzio, L. Glazman, *et al.*, *Phys. Rev. Lett.* **107**, 240501 (2011).

[27] M. H. Devoret and R. J. Schoelkopf, *Science* **339**, 1169 (2013).

[28] D. Leibfried, R. Blatt, C. Monroe, and D. Wineland, *Rev. Mod. Phys.* **75**, 281 (2003).

[29] C. Monroe and J. Kim, *Science* **339**, 1164 (2013).

[30] H. Gan, G. Maslennikov, K.-W. Tseng, C. Nguyen, and D. Matsukevich, *Phys. Rev. Lett.* **124**, 170502 (2020).

[31] H. Buhrman, R. Cleve, J. Watrous, and R. De Wolf, *Phys. Rev. Lett.* **87**, 167902 (2001).

[32] M. A. Nielsen and I. Chuang, “Quantum computation and quantum information,” (2002).

[33] M. Suzuki, *J. Math. Phys.* **32**, 400 (1991).

[34] E. Campbell, *Phys. Rev. Lett.* **123**, 070503 (2019).

[35] J. R. Johansson, P. D. Nation, and F. Nori, *Comput. Phys. Commun.* **183**, 1760 (2012).

[36] A. Kandala, A. Mezzacapo, K. Temme, M. Takita, M. Brink, J. M. Chow, and J. M. Gambetta, *Nature* **549**, 242 (2017).

[37] P. Pfeuty, *Ann. Phys. (N. Y.)* **57**, 79 (1970).

[38] A. Y. Kitaev, *Physics-Uspekhi* **44**, 131 (2001).

[39] P. Jordan and E. P. Wigner, in *The Collected Works of Eugene Paul Wigner* (Springer, 1993) pp. 109–129.

[40] D.-B. Zhang, G.-Q. Zhang, Z.-Y. Xue, S.-L. Zhu, and Z. D. Wang, arXiv:2006.00471 (2020).

[41] M. Dakna, J. Clausen, L. Knöll, and D.-G. Welsch, *Phys. Rev. A* **59**, 1658 (1999).